# Simulations reveal that the HIV-1 gp120-CD4 complex dissociates via complex pathways and is a potential target of the polyamidoamine (PAMAM) dendrimer

Bidisha Nandy, D. Hima Bindu, Narendra M. Dixit, and Prabal K. Maiti

Citation: The Journal of Chemical Physics **139**, 024905 (2013); doi: 10.1063/1.4812801
View online: http://dx.doi.org/10.1063/1.4812801
View Table of Contents: http://scitation.aip.org/content/aip/journal/jcp/139/2?ver=pdfcov
Published by the AIP Publishing

# Simulations reveal that the HIV-1 gp120-CD4 complex dissociates via complex pathways and is a potential target of the polyamidoamine (PAMAM) dendrimer

Bidisha Nandy,[1] D. Hima Bindu,[2] Narendra M. Dixit,[2,a)] and Prabal K. Maiti[1,b)]
[1]*Center for Condensed Matter Theory, Department of Physics, Indian Institute of Science, Bangalore, India*
[2]*Department of Chemical Engineering, Indian Institute of Science, Bangalore, India*

(Received 4 November 2012; accepted 18 June 2013; published online 12 July 2013)

The polyamidoamine (PAMAM) dendrimer prevents HIV-1 entry into target cells in vitro. Its mechanism of action, however, remains unclear and precludes the design of potent dendrimers targeting HIV-1 entry. We employed steered molecular dynamics simulations to examine whether the HIV-1 gp120-CD4 complex is a target of PAMAM. Our simulations mimicked single molecule force spectroscopy studies of the unbinding of the gp120-CD4 complex under the influence of a controlled external force. We found that the complex dissociates via complex pathways and defies the standard classification of adhesion molecules as catch and slip bonds. When the force loading rate was large, the complex behaved as a slip bond, weakening gradually. When the loading rate was small, the complex initially strengthened, akin to a catch bond, but eventually dissociated over shorter separations than with large loading rates. PAMAM docked to gp120 and destabilized the gp120-CD4 complex. The rupture force of the complex was lowered by PAMAM. PAMAM disrupted salt bridges and hydrogen bonds across the gp120-CD4 interface and altered the hydration pattern of the hydrophobic cavity in the interface. In addition, intriguingly, PAMAM suppressed the distinction in the dissociation pathways of the complex between the small and large loading rate regimes. Taken together, our simulations reveal that PAMAM targets the gp120-CD4 complex at two levels: it weakens the complex and also alters its dissociation pathway, potentially inhibiting HIV-1 entry.
 [http://dx.doi.org/10.1063/1.4812801]

## INTRODUCTION

Current antiretroviral therapies curtail the progression of HIV-1 infection but are unable to eradicate the virus. The design of new, more potent drugs remains an important challenge.[1,2] HIV-1 infection of a target cell is preceded by viral attachment to the cell through intermolecular bonds between the viral envelope (Env) protein gp120 and the host cell surface receptor CD4 and subsequently coreceptors CCR5 or CXCR4.[3] Blocking the gp120-CD4-coreceptor interactions can prevent viral entry and, in an advantage over intervention at post-entry steps of the viral replication cycle, protect cells from trespass by HIV. The remarkable variability of HIV-1 Env, however, renders intervention at the level of entry susceptible to failure via viral mutation-induced development of drug resistance. Indeed, no inhibitors of gp120-CD4 binding have been approved for clinical use thus far; an allosteric inhibitor of gp120-CCR5 binding is in clinical use[4] but HIV-1 is known to develop resistance to it.[5] It is of interest therefore to develop HIV-1 entry inhibitors that offer large genetic barriers to resistance.

Dendrimers are highly branched polymers that can be engineered to have various sizes and surface groups, have been shown to be biocompatible, and are being developed for a variety of therapeutic applications.[6–8] Importantly, because of their dendritic structure, they exhibit multivalent binding to their targets, potentially resulting in larger genetic barriers to resistance. Indeed, the fourth generation (G4) polyamidoamine (PAMAM) dendrimer has been shown to be an HIV-1 entry inhibitor with a large genetic barrier and a complex resistance profile.[9,10] Another dendrimer SPL7013 (VivaGel®), which also blocks HIV-1 at the level of entry,[11] has been shown recently to have activity as a vaginal microbicide.[7] Dendrimers thus display remarkable potential as novel HIV-1 entry inhibitors. Yet, their mechanism of action remains poorly understood and precludes rational optimization of their antiviral efficacy.

We employed fully atomistic steered molecular dynamics (SMD) simulations[12] to examine whether the gp120-CD4 complex is a target of the G4 PAMAM dendrimer. Specifically, mimicking single molecule force spectroscopy experiments,[13,14] we orchestrated the dissociation of the gp120-CD4 complex through a controlled external tensile stress, in the presence and in the absence of the dendrimer. The simulations revealed that the gp120-CD4 complex dissociates via complex pathways, defying the standard classification of intermolecular adhesion bonds as *slip* or *catch* bonds.[15,16] In particular, under small force loading rates, the bond initially strengthened, but then eventually dissociated over separations smaller than under large loading rates. When the dendrimer was docked to the gp120-CD4 complex, the complex was weakened and dissociated more readily. The molecular contacts that resulted in the initial strengthening

a)narendra@chemeng.iisc.ernet.in
b)maiti@physics.iisc.ernet.in

 

of the bond under low loading rates were no longer formed. PAMAM altered the dissociation pathway of the complex, potentially compromising the efficiency of HIV-1 entry into target cells. The rest of the paper is organized as follows: In the Methods section, we discuss the details of various methodologies, software, and force fields used to carry out the simulations in the paper. In the Results section, we describe our findings from equilibrium as well as steered MD simulations. Finally, in the Discussion section, we examine the scope of our results in the context of HIV entry and its inhibition.

## METHODS

### Homology modeling of the gp120-CD4 complex

Following Liu *et al.*,[17] the sequence of gp120 (Swiss-Prot accession number P04578)[18] was trimmed to residues 83–492 including the variable loops V3 and V4. The PDB (protein data bank)[19] entries 1G9M[20] and 1CE4[21] were chosen as structural templates of the core gp120 and the V3 loop, respectively, from which the CD4 (chain C), neutralizing antibody Fab 17b (chains L and H), sugar groups, and crystal water molecules were eliminated. Following sequence alignment, models of the gp120 structure were built using the software MODELLER 9 v5.[22] The loop refining module of MODELLER 9 v5 was employed to model the V4 loop. The models were validated using the VERIFY3D software[23] and the model with the highest score selected. The deleted CD4 structure was reintroduced yielding the gp120-CD4 complex that was solvated and employed in our fully atomistic simulations.

### Docking of PAMAM to gp120-CD4 complex

We used ZDOCK,[24] an automated protein docking software, for docking the equilibrated structure of the gp120-CD4 complex and the generation 4 non-protonated PAMAM. The 3D structure of G4 PAMAM was taken from our earlier work.[25–27] We set the gp120-CD4 complex as the receptor and PAMAM as the ligand as inputs to ZDOCK. All the ZDOCK parameters were kept at their default values. ZDOCK generated 10 docked structures of the gp120-CD4-PAMAM complexes and we selected the one with highest score for further simulations and analysis.

### Solvation and equilibration using molecular dynamics (MD) simulation

We performed simulations with the AMBER9.0 software package with the all-atom AMBER03 force field. Using the LEAP module in AMBER, the gp120-CD4 complex was immersed in a water box using the TIP3P model for water.[28] The box dimensions were chosen to ensure that along the pulling direction, the proteins remained in the box throughout. Accordingly, a 20 Å solvation shell was generated around the protein structure along the $y$ and $z$ directions and a 10 Å water shell was generated along the $x$ direction. Some of the water was replaced by 15 $Cl^-$ counter ions to neutralize the positive charge of the proteins. This procedure resulted in a solvated structure containing 118 205 atoms. The solvated structure was subjected to 1000 steps of steepest descent minimization of the potential energy followed by 2000 steps of conjugate gradient minimization. During this minimization process the protein complex was kept fixed in its starting conformation using harmonic constraints with a force constant of 500 kcal/mol/Å$^2$. This allowed the water molecules to reorganize and eliminate unfavorable contacts with the protein structure. The minimized structure was then subjected to 40 ps of MD simulation, using a 2 fs time step for integration. During the MD simulation, the system was gradually heated from 0 to 300 K using weak 20 kcal/mol/Å$^2$ harmonic constraints on the solute to its starting structure. This allowed for slow relaxation of the gp120-CD4 complex. In addition, SHAKE constraints[29] using a geometrical tolerance of $5 \times 10^{-4}$s were imposed on all covalent bonds involving hydrogen atoms which allowed the use of 2 fs time step during MD simulations. Subsequently, MD simulation was performed under constant pressure–constant temperature conditions (NPT), with temperature regulation achieved using the Berendsen weak coupling method[30] (0.5 ps time constant for heat bath coupling and 0.2 ps pressure relaxation time). This was followed by another 5000 steps of conjugate gradient minimization while decreasing the force constant of the harmonic restraints from 20 kcal/mol/Å$^2$ to zero in steps of 5 kcal/mol/Å$^2$. Finally, a 22 ns long MD simulation was carried out using the constant volume–constant temperature (NVT) ensemble. The above protocol produced stable MD trajectories in our earlier studies on biomolecular complexes[31] as also with the gp120-CD4 complex here (Fig. S1 of the supplementary material[47]).

We followed the same protocol to solvate and equilibrate the gp120-CD4-PAMAM complex. DREIDING force field[32] was used to describe the interactions involving PAMAM.

### Steered molecular dynamics (SMD) simulation

In SMD simulations, we pulled the centre-of-mass (COM) of CD4 keeping the COM of gp120 fixed (or vice versa). We followed the same procedure with the gp120-CD4-PAMAM complex. The COM of the pulled protein was harmonically constrained to move with a velocity $v$ in the direction of the line joining the COMs, $\vec{n}$.[33] The COM of the fixed protein was constrained to lie near its initial position with a harmonic spring of constant 1000 kcal/mol/Å$^2$. The effective SMD potential is given by $U(\vec{r}) = \frac{k}{2}[vt - (\vec{r} - \vec{r}_0).\vec{n}]^2$, and the resulting pulling force, $\vec{F} = -\nabla U$, where $k$ is the force constant, and $\vec{r}$ and $\vec{r}_0$ are the positions of the pulled protein at time $t$ and at the initial time. If the proteins moved away from each other along the reaction coordinate, $\vec{r} - \vec{r}_0$ increased and the force decreased. If the pulling force did not displace the proteins, the force increased with $t$. The resulting trajectories of the complex were recorded yielding, in particular, force versus extension curves for each pulling velocity chosen. The SMD simulations with gp120-CD4 were performed with AMBER9.0. With PAMAM, the number of atoms in the system nearly doubled. We therefore used NAMD[34] for the SMD simulations with PAMAM, given its computational efficiency, again with the same force fields. In changing the software from AMBER to NAMD we have taken enough care to use

similar simulation conditions and ensured that we get similar results. For comparison, we have shown force versus distance plots from the SMD runs using both AMBER and NAMD at two different loading rates in Fig. S3 of the supplementary materials,[47] which demonstrates that the two softwares can be used interchangeably.

### MMPB/GBSA energy

The MM-PB/GB-SA method[35] (MM: Molecular Mechanics; PB: Poisson-Boltzmann; GB: Generalized Born; SA: Surface Area) was used to calculate the binding energy of the gp120-CD4 complex: $\Delta G_{bind} = G_{complex} - G_{gp120} - G_{CD4}$. The binding energy can also be written as $\Delta G_{bind} = \Delta H_{bind} - T\Delta S_{bind}$, where $\Delta H_{bind} = \Delta E_{ele} + \Delta E_{vdw} + \Delta E_{\text{int}} + \Delta E_{sol}$ is the sum of the changes in the electrostatic energy, $\Delta E_{ele}$, non-bond van der Waals energy, $\Delta E_{vdw}$, the internal energy from bonds, angles, and torsions, $\Delta E_{\text{int}}$, and the contribution from the solvent, $\Delta E_{sol}$. The latter contribution, $\Delta E_{sol} = \Delta E_{es} + \Delta E_{nes}$, is the sum of the electrostatic energy, $\Delta E_{es}$, calculated using the Poisson-Boltzmann (PB) method, and the non-electrostatic energy, $\Delta E_{nes}$, calculated as $\gamma SASA + \beta$, where $\gamma = 0.00542$ kcal/Å$^2$ is the surface tension, $\beta = 0.92$ kcal/mol, and *SASA* is the solvent-accessible surface area of the molecule.[36] $T\Delta S_{bind}$, the solute entropy, was ignored in our present study. The time evolution of the binding free energies of the gp120-CD4 complex before pulling were determined using gas-phase energies (MM) and solvation free energies following the Generalized Born model (GB/SA) analysis for snapshots obtained from a total of 22 ns of simulation (Fig. S1(b) of the supplementary material[47]).

### Number of intermolecular contacts

The number of intermolecular contacts was calculated using the following criteria: if any atom in CD4 fell within 3 Å of any atom in gp120, then the two atoms were considered a contact between the two molecules. From this contact analysis we identified each atom of gp120 and CD4 responsible for making contacts between the two molecules. Further, we analyzed the contacts and identified the residues that resulted in additional contacts when the binding energy attained a maximum in the slow pulling rate regime (separation ~1.8 Å).

### Interfacial cavities and hydration

We identified the known boundary residues of the hydrophobic cavity, Trp 112, Val 155, etc.,[20] and using the Visual MD (VMD)[37] TCL script we identified the centre of the cavity, which is known to be roughly spherical.[20]. We counted the number of water molecules within ~8 Å from the centre of the cavity as a measure of the hydration level of the cavity.

The hydrophilic cavity is non-spherical.[20] Here, we again identified the residues forming the cavity, Ala 281, Ser 364, etc.,[20] and counted the number of water molecules within a 3 Å shell from these residues using the VMD TCL script as an estimate of the water molecules in the shell.

### Salt bridges and hydrogen bonds

We used the salt-bridge analysis tool of VMD and identified all salt-bridges between the oxygen atoms of acidic residues and the nitrogen atoms of basic residues within a distance 3.4 Å across the gp120-CD4 interface. We identified the hydrogen bonds between gp120 and CD4 using the hydrogen bonds analysis routine in VMD with a donor acceptor distance cut-off of 3.0 Å and an angle cut-off of 20°.

## RESULTS

### Structure of the gp120-CD4 complex

We built the structure of gp120 using homology modeling,[17] complexed it with CD4 based on the crystal structure of the gp120-CD4 complex, solvated the complex with water, added $Cl^-$ ions for charge neutralization, and performed molecular dynamics (MD) simulations of the resulting structure containing 118205 atoms (Fig. 1(a)) at 300 K in the absence of any external force (Methods). The complex displayed a small root-mean-square-displacement (RMSD) from the crystal structure[20] (Fig. S1 of the supplementary materials[47]). We computed the enthalpy of the complex and found it to be $-52 \pm 11$ kcal/mol, in close agreement with the experimental value of $-62$ kcal/mol,[38] validating our structure of the gp120-CD4 complex. We employed two snapshots of the complex, one after 1 ns and the other after 19 ns of MD simulation, respectively, as initial configurations for SMD simulations.

### Dissociation of the gp120-CD4 complex

In SMD, the dissociation of a complex is guided by an external force.[12] We applied a force through a harmonic spring on the center-of-mass (COM) of CD4 keeping the COM of gp120 fixed. (Applying the force on gp120 instead yielded similar results (Fig. S2 of the supplementary material[47])). We chose the line joining the centers-of-mass as the reaction coordinate and modulated the force to achieve a constant pulling velocity, $\nu$ (see the Methods section). We performed simulations with $\nu$ spanning two orders of magnitude, ranging from 0.0017 Å/ps to 0.17 Å/ps.

At any $\nu$, as the separation between gp120 and CD4 increased, the force applied increased, indicating the increasing resistance to pulling the complex offered as it was stretched (Fig. 1(b)). Beyond a certain separation, however, the force decreased, signifying the onset of bond dissociation and mechanical yielding. Bond rupture was complete by a separation of 10–20 Å (Fig. 1(c)), beyond which the force decreased to zero. This force-extension profile was qualitatively similar to that observed in single molecule pulling experiments.[13,14]

### Complex dissociation pathways

We analyzed the force-extension data and determined the rupture (or maximum) force, $F$, the force loading rate at rupture, $r_f$, and the separation at rupture for each of our simulations (Figs. S4 and S5 of the supplementary material[47]). The

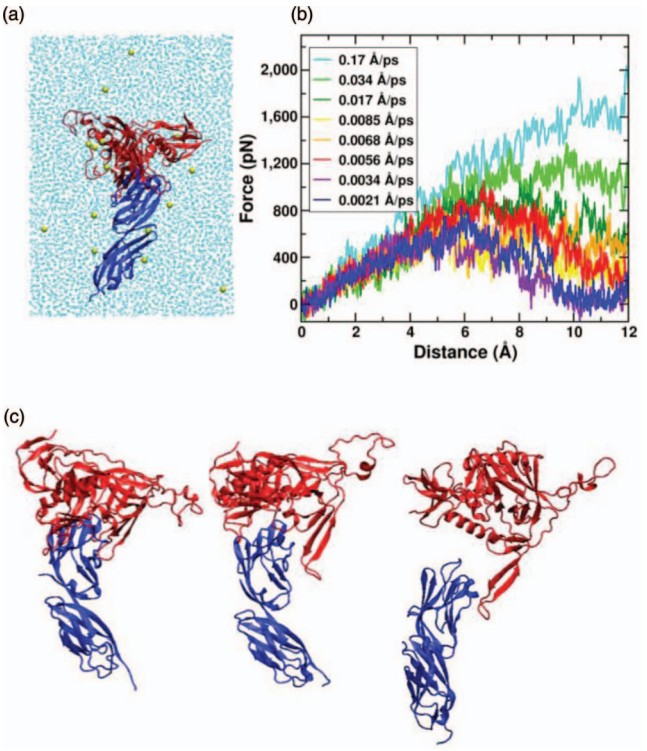


FIG. 1. SMD simulations of the dissociation of the gp120-CD4 complex. (a) The simulation system comprising gp120 (red), CD4 (blue), $Cl^-$ ions (yellow), and water molecules (cyan background). (b) Force versus extension curves for different pulling velocities. (c) Snapshots of the initial structure, the structure at bond rupture (separation 9.4 Å), and well after bond rupture (separation 22.7 Å) for $\nu = 0.0021$ Å/ps.

rupture force, loading rate, and the separation at rupture for a given pulling run were computed as follows: Running averages were computed with appropriate block sizes for each pulling velocity (Fig. 2). The region approaching rupture was fit using a straight line. The slope of this straight line multiplied by the pulling velocity gave the loading rate (pN/ps) at rupture. The maximum of the running average of the force gave the rupture force. The extension at the maximum gave the separation at rupture. We found that each of these quantities increased with $\nu$ (Figs. 3(a) and S6 of the supplementary material[47]). Interestingly, we found two regimes of the dependence of $F$ on $\nu$ (Fig. 3(a)) or $r_f$ (Fig. 3(a) inset). For large $r_f$, >1 pN/ps, $F$ increased linearly with $r_f$; whereas for small $r_f$, <1 pN/ps, $F$ was weakly dependent on $r_f$. Similar regimes were observed experimentally not only with HIV-1 gp120-CD4[13] but also with actomyosin.[39] Further, $F$ was lower with the initial configuration after 19 ns of MD than after 1 ns (Fig. 3(a)), in agreement with the spontaneous destabilization of the gp120-CD4 complex observed experimentally.[14]

To further characterize the two regimes, we computed the number of contacts, $C$, between gp120 and CD4, and the instantaneous binding energy, $E$, during the simulations (Figs. 3(b)). In the large $r_f$ regime, $C$ decreased gradually and $E$ increased (implying weakening of the complex), both eventually reaching zero at complete dissociation. Surprisingly, in the low $r_f$ regime, $C$ initially increased (until a separation of ~2 Å) and $E$ declined, indicating strengthening of the complex. This strengthening was associated with increases in the RMSD of gp120 and CD4 (Fig. S7 of the supplementary material[47]), indicating that slow pulling allowed conformational changes in both proteins that led to the formation of additional intermolecular contacts. We examined the contacts formed and found that residues Asn 280 and Ala 281 in gp120 were among those that formed additional contacts in the low but not the high $r_f$ regime (Fig. 3(d) and Table S1 of the supplementary material[47]). Subsequently, $C$ declined and $E$ increased until complete dissociation. Remarkably, complete dissociation occurred at separations (~10 Å) much smaller than in the high $r_f$ regime (~15–20 Å). Thus, despite the initial strengthening, the complex dissociated over smaller separations when $r_f$ was low. In other words, efficient dissociation here involved the formation of new intermolecular contacts upon the application of a gradual tensile force. This complex dissociation behavior was robust and occurred with both the initial configurations employed (Fig. S8 of the supplementary material[47]). The gp120-CD4 complex is thus distinct from typical slip or catch bonds and may embody a design principle that may facilitate viral entry (see Discussion). We examined next the influence of a dendrimer.

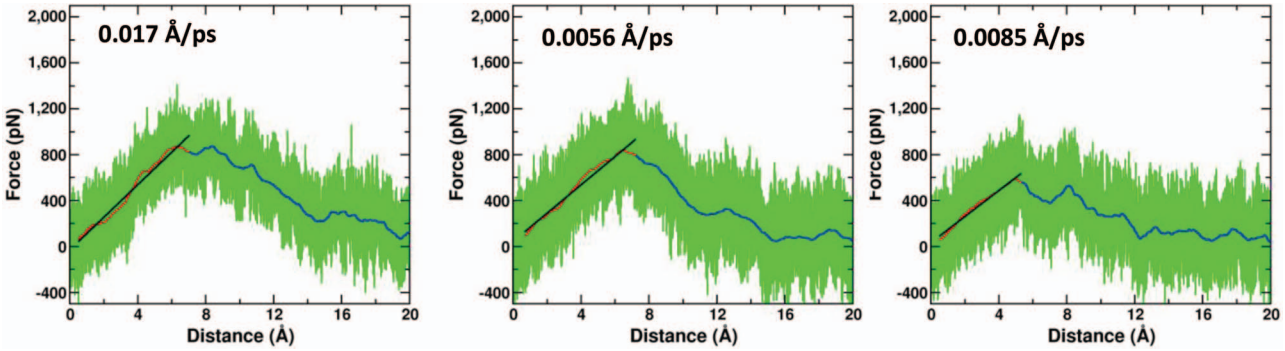


FIG. 2. Force versus extension profiles (green) of the gp120-CD4 complex for three different pulling velocities with the initial structure following 19 ns of MD simulation.Running averages were computed with appropriate block sizes for each pulling velocity (blue line). The region approaching rupture (red line) was fit using a straight line (black line). The slope of this straight line multiplied by the pulling velocity gave the loading rate (pN/ps) at rupture. The maximum of the running average of the force (blue) gave the rupture force.

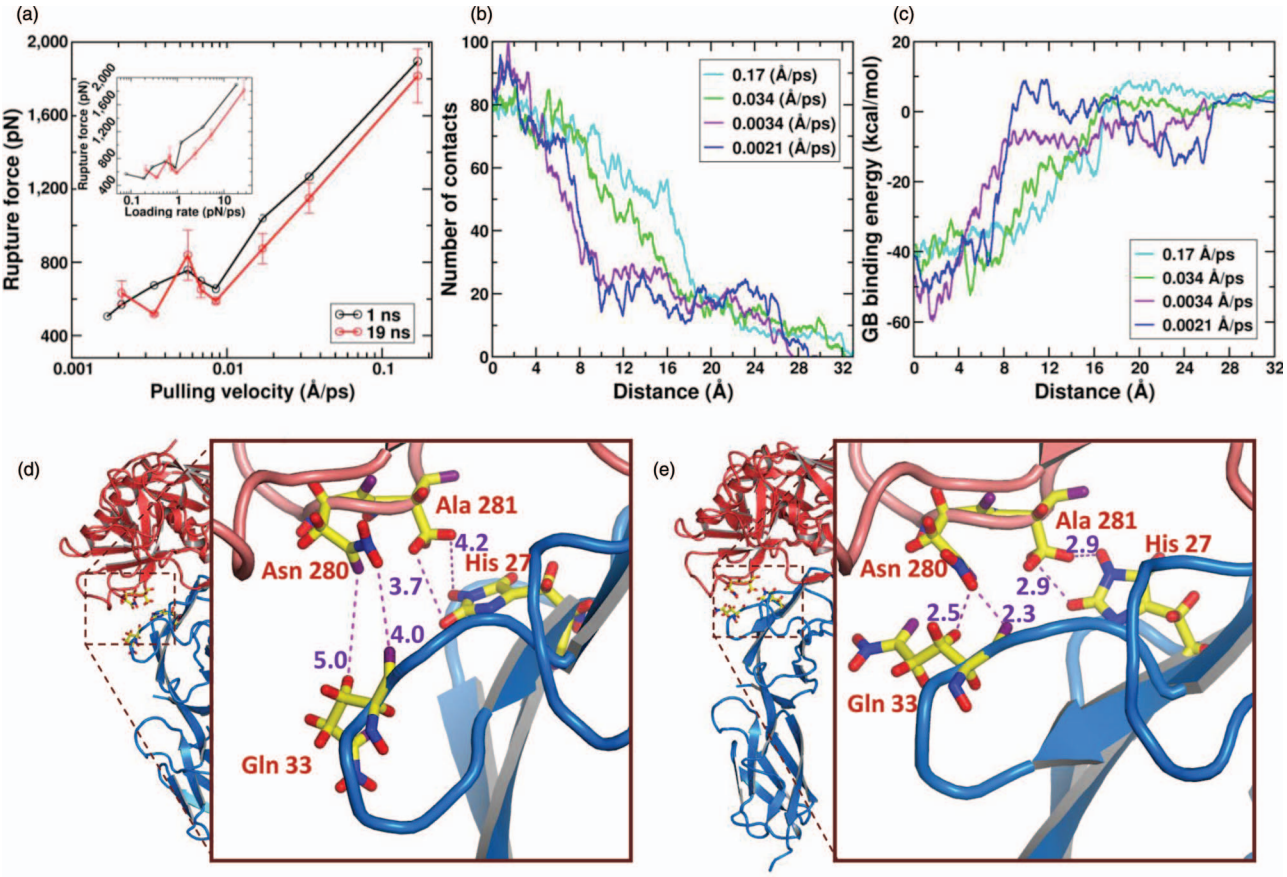


FIG. 3. Dissociation pathways of the gp120-CD4 complex. (a) Two regimes of the dependence of $F$ on $v$ with initial configurations obtained after 1 ns (black line) and 19 ns (red line) of MD and the corresponding dependence of $F$ on $r_f$ (inset). Error bars are standard deviations obtained from four different realizations of our simulations at each pulling velocity. Time-evolution of (b) the number of contacts and (c) the binding energy for four pulling velocities, two each in the large (cyan and green) and the small (purple and blue) $r_f$ regimes. Snapshots indicating new contacts formed by residues Asn 280 and Ala 281 in the small $r_f$ regime ($v = 0.0034$ Å/ps) (e) but not in the high $r_f$ regime ($v = 0.034$ Å/ps) (d). Note that an inter-atomic separation of 3 Å or less indicates a contact.

### Structure of the gp120-CD4-PAMAM ternary complex

We docked PAMAM to the gp120-CD4 complex and found that PAMAM binds to gp120. We solvated the resulting ternary complex with water, added $Cl^-$ ions for charge neutralization, and performed MD simulations of the resulting structure containing 205 703 atoms at 300 K (Methods) in the absence of any external force. The complex displayed a small RMSD from the initial structure (Fig. S9 of the supplementary material[47]). We employed the structure of the complex after 9 ns of MD as the initial configuration for SMD simulations (Fig. 4(a)).

### PAMAM weakens the gp120-CD4 complex

We performed SMD simulations at values of $v$ close to those employed above. The force-extension profiles (Fig. 4(b) and Fig. S10 of the supplementary material[47]) were similar to those obtained without PAMAM (Fig. 1(b)), eventually leading to complete dissociation of the gp120-CD4 complex (Fig. 4(c)). Throughout the simulations, PAMAM remained bound to gp120 reaffirming the stability of the gp120-PAMAM complex. Interestingly, we found that $F$ was lower in the presence of PAMAM than in the absence of PAMAM (Fig. 5(a)), indicating that PAMAM destabilized the gp120-CD4 complex. Interestingly, when $F$ was plotted against $r_f$ instead of $v$, the data with and without PAMAM collapsed onto the same scaling regimes (Fig. 5(a) inset). Thus, for any $v$, PAMAM effectively lowered $r_f$ and hence $F$. PAMAM may thus inhibit viral entry by weakening gp120-CD4 association.

### PAMAM alters the dissociation pathway of the gp120-CD4 complex

$F$ versus $r_f$ data, obtained by analyzing the force-extension profiles (Fig. S10 of the supplementary material[47]), did show two regimes of dissociation (Fig. 5(a)). The complex dissociation of the low $r_f$ regime, however, was subdued. In the high $r_f$ regime, $C$ decreased gradually and $E$ increased, both eventually reaching zero at complete dissociation (Figs. 5(b)), in a manner similar to the case without PAMAM (Figs. 3(b)). In the low $r_f$ regime, however, the initial rise in $C$ and the concomitant decline in $E$ were suppressed compared to the case without PAMAM. Indeed, except for the case where $v = 0.0033$ Å/s, $C$ did not display a significant increase following the onset of pulling, indicating similar behavior in both the low and the high $r_f$ regimes. Interestingly, the RMSD of gp120 and CD4 indicate that while gp120 continued to exhibit increased conformational changes in the low

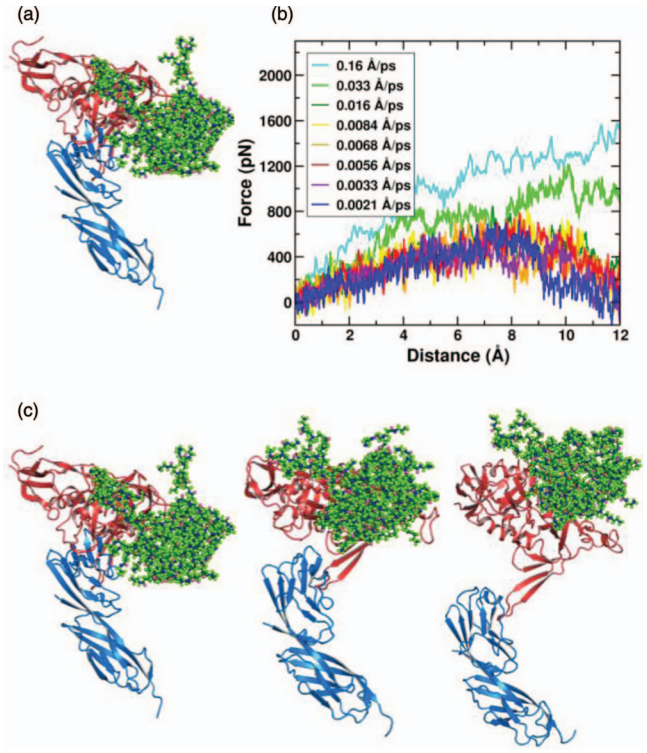


FIG. 4. SMD simulations of the gp120-CD4 complex dissociation in the presence of PAMAM. (a) The simulation system comprising gp120 (red), CD4 (blue), PAMAM (green), $Cl^-$ ions (yellow), and water molecules (not shown). (b) Force versus extension curves for different pulling velocities. (c) Snapshots of the initial structure, the structure at bond rupture (separation 6.6 Å), and well after bond rupture (separation 23.8 Å) for $\nu = 0.0068$ Å/ps.

$r_f$ regime, conformational changes of CD4 were considerably restricted in the presence of PAMAM and were similar in the two regimes (Fig. S12 of the supplementary material[47]), suggesting that PAMAM potentially precluded the conformational changes in the proteins that led to the formation of additional contacts with low $r_f$. Indeed, residues Asn 280 and Ala 281 in gp120, where additional contacts were formed in the absence of PAMAM, now formed no additional contacts (Table S2 of the supplementary material[47]). Additional contacts were formed at another residue, Cys 126, in gp120 (Fig. 5(d)), but the distinction between the dissociation pathways in the two regimes was less evident. The complex dissociated over roughly similar separations in both the $r_f$ regimes (Figs. 5(b) and S13 of the supplementary material[47]). PAMAM thus suppressed the complex dissociation pathway of the low $r_f$ regime.

### PAMAM modulates the interactions of hydrophobic and hydrophilic residues in gp120 with CD4

To further characterize the influence of PAMAM on gp120-CD4 interactions, we examined the residues at which gp120 and CD4 formed contacts in the absence and presence of PAMAM at a separation of ~2 Å during pulling. We found differences in the contacts formed at 9 gp120 residues due to PAMAM (Table I). In particular, Ser 195, which formed several contacts with CD4 in the absence of PAMAM formed no contacts in the presence of PAMAM. At the same time, Leu 125, which formed no contacts in the absence of PAMAM formed new contacts in the presence of PAMAM. Of the 9 gp120 residues that were influenced by PAMAM, 4 were hydrophobic and 5 were hydrophilic. Intriguingly, 3 of the 4 hydrophobic residues formed more contacts with CD4 in the presence of PAMAM than in its absence, and 3 of the 5 hydrophilic residues formed fewer contacts in the presence of PAMAM. Thus, PAMAM tended to increase the contacts made by hydrophobic residues on gp120 with CD4 and reduce those made by hydrophilic residues.

### PAMAM alters the hydration of the hydrophobic interfacial cavity

Given that PAMAM altered the binding patterns of hydrophobic and hydrophilic residues differently, we asked whether PAMAM also altered the water content in hydrophilic and hydrophobic regions of the gp120-CD4 interface differently. Specifically, we examined the water content in the two major cavities, one of which is hydrophobic and the other hydrophilic, in the gp120-CD4 interface.[20] We found that in the presence of PAMAM, whereas the hydration of the large hydrophilic cavity remained largely unaffected, the hydration of the hydrophobic cavity surrounding the Phe 43 residue of CD4 decreased. Whereas 8–10 water molecules existed in the cavity in the absence of PAMAM (Fig. 6(a)), the number reduced to 6–8 in the presence of PAMAM (Fig. 6(b)).

### PAMAM disrupts salt bridges across gp120 and CD4

We examined next the salt bridges formed across the gp120-CD4 interface in the presence and absence of PAMAM both before and during pulling. We found five salt bridges across the gp120-CD4 interface in the absence of PAMAM before pulling (Table S3 of the supplementary material[47]). With PAMAM, two of these salt bridges, namely, the ones between Lys 22 of CD4 and Glu 102 of gp120 and between Lys 29 of CD4 and Asp 279 of gp120, ceased to exist and two additional salt bridges became weak in that the separation between the residues across which the salt bridges were formed increased. All the five salt bridges were also observed during pulling in the absence of PAMAM. With PAMAM, however, again, two salt bridges were absent and two others were either absent or weakened. Salt bridges are known to be a key factor underlying the stability of protein structures. PAMAM thus weakens the gp120-CD4 complex by breaking and/or weakening salt bridges across the gp120-CD4 interface.

### PAMAM disrupts hydrogen bonds across gp120 and CD4 and alters their patterns of dissociation during pulling

Finally, we examined the influence of PAMAM on the hydrogen bonds formed across gp120 and CD4. Before pulling, we found 8 hydrogen bonds across the gp120-CD4 interface (Table S4 of the supplementary material[47]). With PAMAM, three of these bonds were absent. In addition, three

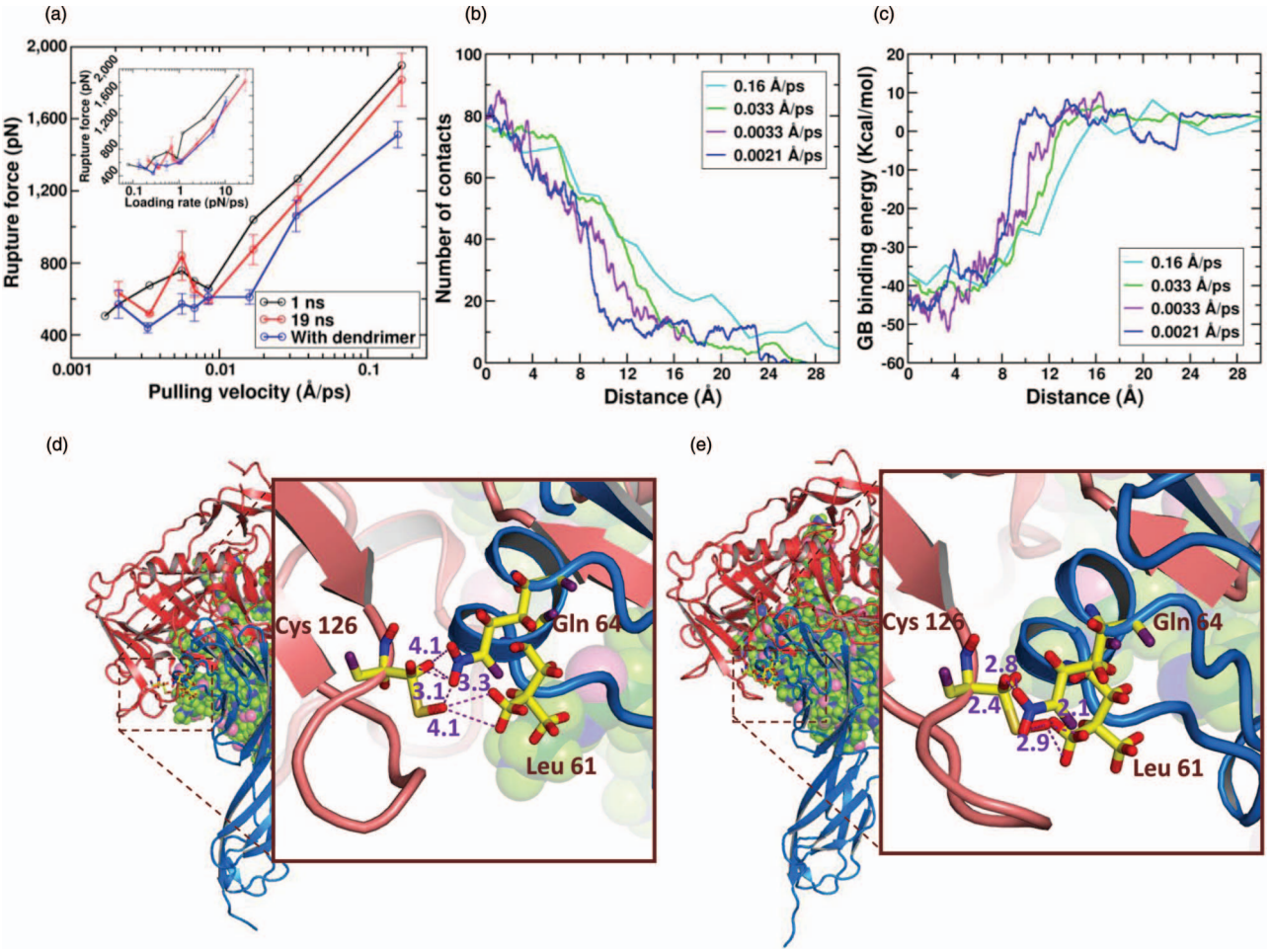


FIG. 5. Dissociation pathways of the gp120-CD4 complex in the presence of PAMAM. (a) The dependence of $F$ on $v$ and $r_f$ (inset) with PAMAM (blue line) compared with that without PAMAM (black and red lines; see Fig. 1). Error bars are standard deviations from four realizations of our simulations at each $v$. Time-evolution of (b) the number of contacts and (c) the binding energy for four pulling velocities, two each in the large (cyan and green) and the small (purple and blue) $r_f$ regimes. Snapshots indicating new contacts formed by the residue Cys 126 in the small $r_f$ regime ($v = 0.0033$ Å/ps) (e) but not in the high $r_f$ regime ($v = 0.033$ Å/ps) (d). Note that an inter-atomic separation of 3 Å or less indicates a contact.

other hydrogen bonds were weak, in that they were found to occur over a smaller fraction of sampling times. PAMAM thus weakened the gp120-CD4 complex also by suppressing hydrogen bond formation across the proteins.

Intriguingly, the patterns of breaking of these hydrogen bonds were different in the low and high $r_f$ regimes with and without PAMAM. In the absence of PAMAM, five of the hydrogen bonds dissociated significantly more rapidly in the low $r_f$ regime than in the high $r_f$ regime (Table S4 of the supplementary material[47]). For instance, the hydrogen bond across the Arg 59 residue of CD4 and Asp 368 residue on gp120 was found to occur ∼20% of the time during pulling in the high $r_f$ regime versus ∼10% in the low $r_f$ regime. Similarly, the bond between Ser 42 and Met 426 existed ∼30% and ∼4% of the time, respectively. The rapid dissociation of these hydrogen bonds in the low $r_f$ regime may underlie the efficient dissociation of the gp120-CD4 complex in this regime. The presence of PAMAM reversed these trends. The hydrogen bond between Arg 59 and Asp 368 now existed for ∼3% of the time during pulling in the high $r_f$ regime versus ∼10%–20% in the low $r_f$ regime. The bond between Ser 42 and Met 426 did not occur at all in the high $r_f$ regime and occurred for <0.2% of the time in the low $r_f$ regime, explaining at least in part how PAMAM suppressed the differences between the high and low $r_f$ regimes.

In summary, PAMAM destabilizes the gp120-CD4 complex, alters its dissociation pathway, and potentially compromises HIV-1 entry into target cells. The influence of PAMAM is mediated through altered hydration pattern of a gp120-CD4 interfacial cavity, an increase (decrease) in the interactions of hydrophobic (hydrophilic) gp120 residues with CD4, and the weakening of salt-bridges and hydrogen bonds across gp120 and CD4.

## DISCUSSION

The tunability of their size, shape, and surface groups, the ease of their synthesis, their multivalent binding to their targets, and the resulting large genetic barrier to the development of drug resistance they offer renders dendrimers a unique class of candidate drug molecules for targeting rapidly evolving pathogens such as HIV. Using fully atomistic SMD simulations, we show here that the dendrimer PAMAM[9] binds to the HIV-1 gp120-CD4 complex, weakens the complex, and alters

TABLE I. Inter-atomic contacts between gp120 and CD4 influenced by PAMAM. The number of inter-atomic contacts between gp120 residues and CD4 in the low and high loading rate regimes in the absence and presence of PAMAM, determined at a separation of ∼1.8 Å during pulling. The Kyte-Doolittle hydrophobicity index of the residues is mentioned, where positive values indicate hydrophobicity and negative values indicate hydrophilicity. The detailed lists of atomic contacts are in Tables S1 and S2.[47]

| | | Number of contacts | | | |
|---|---|---|---|---|---|
| | | Without PAMAM | | With PAMAM | |
| gp120 residue | Hydrophobicity Index | Low $r_f$ | High $r_f$ | Low $r_f$ | High $r_f$ |
| Leu 125 | 3.8 | 0 | 0 | 3–7 | 1–2 |
| Cys 126 | 2.5 | 0–4 | 0 | 9–12 | 2–6 |
| Ser 195 | − 0.8 | 2–6 | 2–4 | 0 | 0 |
| Asn 280 | − 3.5 | 5–7 | 2–3 | 2–3 | 3–5 |
| Ala 281 | 1.8 | 8–10 | 2–5 | 2–3 | 1–3 |
| Lys 282 | − 3.9 | 1–4 | 1–2 | 2–5 | 4–6 |
| Asn 425 | − 3.5 | 8 | 4–8 | 2 | 2 |
| Val 430 | 4.2 | 5–6 | 3–4 | 8–10 | 6–7 |
| Asp 474 | − 3.5 | 2–6 | 4–6 | 7 | 6–7 |

its dissociation pathways. PAMAM may thus be representative of a potentially new class of drug molecules that blocks HIV-1 entry into cells by targeting the gp120-CD4 complex.

Biological adhesion molecules are classified as slip or catch bonds depending on their response to an applied tensile stress.[15,16] Slip bonds steadily weaken whereas catch bonds strengthen under the influence of an external tensile stress. We found that the gp120-CD4 complex is neither a slip nor a catch bond. It can dissociate via two distinct pathways in response to an applied tensile stress depending on the force loading rate, $r_f$. With large $r_f$, the complex continuously destabilizes, indicating slip behavior. With small $r_f$, the complex initially stabilizes, indicating catch behavior, but then dissociates over shorter separations than with large $r_f$. The complex is thus also distinct from the recently identified "catch-slip" bonds that behave as catch bonds under small stresses and slip bonds under large stresses.[39,40] With the adhesion molecule P-selectin, rapid dissociation with small $r_f$ was observed but an initial strengthening of the bond was not reported.[41] Uniquely, the gp120-CD4 complex initially strengthens and then rapidly yields with small $r_f$. Thus, dissociation of the complex along this pathway involves the formation of new intermolecular contacts upon the application of a small separating force. When the pulling direction is distinct from the spontaneous dissociation reaction coordinate, the formation of new contacts induced by the applied force is expected, but such contacts typically hinder bond dissociation.[42] Here, dissociation occurs over shorter separations indicating that the new contacts, counter-intuitively, facilitate eventual dissociation.

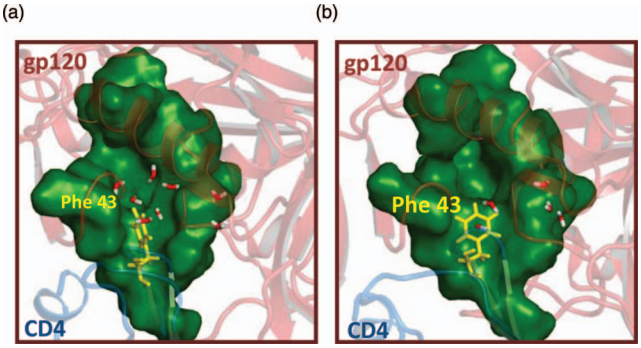


FIG. 6. Hydration of the hydrophobic cavity of gp120. The hydrophobic cavity of gp120, in the middle of the green region surrounding the Phe 43 residue of CD4 (yellow) contains more water molecules (red and white) in the absence of PAMAM (a) than in the presence of PAMAM (b).

SMD simulations have been developed recently as a tool for screening drug candidates.[43,44] Candidates that bind tightly to their intended targets are identified as potential drug candidates. For this, efficient dissociation pathways are identified using short simulations along randomly chosen pulling directions and rejecting directions where the free energy initially rises.[44] Our simulations suggest that an initial rise in the free energy does not necessarily imply an inefficient dissociation pathway. Rejecting such pathways may thus result in the selection of candidates that may eventually not bind as tightly to their targets as expected, thus increasing false positives.

The observed response of the gp120-CD4 complex may be designed to benefit HIV-1. Efficient viral entry into target cells appears to place conflicting demands on the mechanical properties of the entry receptor complexes. On the one hand, the complexes must resist dissociation to ensure attachment of the virus to the target cell until entry can occur. On the other hand, limited dissociation may grant the virus mobility on the cell surface to scan the cell surface for the requisite receptors and thereby expedite entry. Multiple gp120-CD4-coreceptor complexes are thought to be necessary for viral entry.[45,46] The gp120-CD4 complex may continually experience small stresses over short durations due to the natural fluctuations of the lipid membranes in which gp120 and CD4 are anchored. Strengthening of the complex in response to such stresses ensures lasting viral attachment to target cells. Continued stress on the complex may be due to an energetically unfavorable location of the virion or proximity to CCR5, which destabilizes the complex.[14] The complex then rapidly dissociates, potentially facilitating movement to more favorable locations on the cell and/or CCR5 binding. The latter movement may be aided by the spontaneous destabilization of the gp120-CD4 complex.

Our simulations are in qualitative agreement with recent single molecule force spectroscopy experiments.[13,14] In particular, the gp120-CD4 complex was observed to exhibit two distinct regimes of dissociation depending on the loading rate, $r_f$.[13] Further, the complex appeared to destabilize spontaneously after formation.[14] Quantitative comparisons with these experiments are precluded by the several orders of magnitude faster pulling velocities employed in our simulations to keep the simulations computationally feasible. Going beyond experimental findings, our simulations elucidate the complex dissociation pathways of the gp120-CD4 complex and the molecular underpinnings of its mechanical properties.[13,14] Our simulations identified the residues that were responsible for the initial stabilization of the complex in the small $r_f$ regime. We found that residues Asn 280 and Ala 281 in gp120 were among those that formed additional contacts in the small but not the large $r_f$ regime. Preventing the formation of these contacts may thus suppress, if not eliminate, the complex

dissociation pathway of the small $r_f$ regime. Indeed, dissociation of the gp120-CD4 complex when PAMAM was docked to gp120 prevented the formation of these contacts and suppressed the distinction in the dissociation pathways between the large and small $r_f$ regimes. In addition, PAMAM altered the hydration level of the hydrophobic cavity and reduced the number and/or strength of salt bridges and hydrogen bonds across the gp120-CD4 interface, thus weakening the complex. Indeed, the rupture force was significantly smaller in the presence of PAMAM than in its absence. Taken together, our study suggests that PAMAM, which has been shown experimentally to inhibit HIV-1 entry,[9] may act by targeting the gp120-CD4 complex at two levels: it destabilizes the complex and by altering its dissociation pathway compromises its mechanical properties designed to facilitate entry.

## ACKNOWLEDGMENTS

This work was funded by the Department of Science & Technology (DST) Mathematical Biology Initiative at the Indian Institute of Science, Bangalore.

[1]Y. Mehellou and E. De Clercq, J. Med. Chem. **53**, 521 (2010).
[2]B. Berkhout and R. W. Sanders, Antiviral Res. **92**, 7 (2011).
[3]D. C. Chan and P. S. Kim, Cell **93**, 681 (1998).
[4]P. Dorr, M. Westby, S. Dobbs, P. Griffin, B. Irvine, M. Macartney, J. Mori, G. Rickett, C. Smith-Burchnell, C. Napier, R. Webster, D. Armour, D. Price, B. Stammen, A. Wood, and M. Perros, Antimicrob. Agents Chemother. **49**, 4721 (2005).
[5]M. Roche, M. Jakobsen, A. Ellett, H. Salimiseyedabad, B. Jubb, M. Westby, B. Lee, S. Lewin, M. Churchill, and P. Gorry, Retrovirology **8**, 89 (2011).
[6]V. Gajbhiye, V. K. Palanirajan, R. K. Tekade, and N. K. Jain, J. Pharm. Pharmacol. **61**, 989 (2009).
[7]C. F. Price, D. Tyssen, S. Sonza, A. Davie, S. Evans, G. R. Lewis, S. Xia, T. Spelman, P. Hodsman, T. R. Moench, A. Humberstone, J. R. A. Paull, and G. Tachedjian, PLoS ONE **6**, e24095 (2011).
[8]T. S. Barata, I. Teo, S. Brocchini, M. Zloh, and S. Shaunak, PLoS Comput. Biol. **7**, e1002095 (2011).
[9]M. Witvrouw, V. Fikkert, W. Pluymers, B. Matthews, K. Mardel, D. Schols, J. Raff, Z. Debyser, E. De Clercq, G. Holan, and C. Pannecouque, Mol. Pharmacol. **58**, 1100 (2000).
[10]A. Hantson, V. Fikkert, B. Van Remoortel, C. Pannecouque, P. Cherepanov, B. Matthews, G. Holan, E. De Clercq, A. M. Vandamme, Z. Debyser, and M. Witvrouw, Antivir. Chem. Chemother. **16**, 253 (2005).
[11]D. Tyssen, S. A. Henderson, A. Johnson, J. Sterjovski, K. Moore, J. La, M. Zanin, S. Sonza, P. Karellas, M. P. Giannis, G. Krippner, S. Wesselingh, T. McCarthy, P. R. Gorry, P. A. Ramsland, R. Cone, J. R. A. Paull, G. R. Lewis, and G. Tachedjian, PLoS ONE **5**, e12309 (2010).
[12]M. Sotomayor and K. Schulten, Science **316**, 1144 (2007).
[13]M. I. Chang, P. Panorchan, T. M. Dobrowsky, Y. Tseng, and D. Wirtz, J. Virol. **79**, 14748 (2005).
[14]T. M. Dobrowsky, Y. Zhou, S. X. Sun, R. F. Siliciano, and D. Wirtz, J. Virol. **82**, 7022 (2008).
[15]E. Evans and K. Ritchie, Biophys. J. **72**, 1541 (1997).
[16]W. E. Thomas, E. Trintchina, M. Forero, V. Vogel, and E. V. Sokurenko, Cell **109**, 913 (2002).
[17]S. Q. Liu, S. X. Liu, and Y. X. Fu, J. Mol. Model. **13**, 411 (2007).
[18]A. Bairoch, U. Consortium, L. Bougueleret, S. Altairac, V. Amendolia, A. Auchincloss, G. Argoud-Puy, K. Axelsen, D. Baratin, M. C. Blatter, B. Boeckmann, J. Bolleman, L. Bollondi, E. Boutet, S. B. Quintaje, L. Breuza, A. Bridge, E. Decastro, L. Ciapina, D. Coral, E. Coudert, I. Cusin, G. Delbard, D. Dornevil, P. D. Roggli, S. Duvaud, A. Estreicher, L. Famiglietti, M. Feuermann, S. Gehant, N. Farriol-Mathis, S. Ferro, E. Gasteiger, A. Gateau, V. Gerritsen, A. Gos, N. Gruaz-Gumowski, U. Hinz, C. Hulo, N. Hulo, J. James, S. Jimenez, F. Jungo, V. Junker, T. Kappler, G. Keller, C. Lachaize, L. Lane-Guermonprez, P. Langendijk-Genevaux, V. Lara, P. Lemercier, V. Le Saux, D. Lieberherr, T. D. Lima, V. Mangold, X. Martin, P. Masson, K. Michoud, M. Moinat, A. Morgat, A. Mottaz, S. Paesano, I. Pedruzzi, I. Phan, S. Pilbout, V. Pillet, S. Poux, M. Pozzato, N. Redaschi, S. Reynaud, C. Rivoire, B. Roechert, M. Schneider, C. Sigrist, K. Sonesson, S. Staehli, A. Stutz, S. Sundaram, M. Tognolli, L. Verbregue, A. L. Veuthey, L. Yip, L. Zuletta, R. Apweiler, Y. Alam-Faruque, R. Antunes, D. Barrell, D. Binns, L. Bower, P. Browne, W. M. Chan, E. Dimmer, R. Eberhardt, A. Fedotov, R. Foulger, J. Garavelli, R. Golin, A. Horne, R. Huntley, and J. Jacobsen, Nucleic Acids Res. **37**, D169 (2009).
[19]H. Berman, J. Westbrook, Z. Feng, G. Gilliland, T. Bhat, H. Weissig, I. Shindyalov, and P. Bourne, Nucleic Acids Res. **28**, 235 (2000).
[20]P. D. Kwong, R. Wyatt, J. Robinson, R. W. Sweet, J. Sodroski, and W. A. Hendrickson, Nature (London) **393**, 648 (1998).
[21]W. Vranken, M. Budesinsky, F. Fant, K. Boulez, and F. Borremans, FEBS Lett. **374**, 117 (1995).
[22]A. Sali and T. L. Blundell, J. Mol. Biol. **234**, 779 (1993).
[23]D. Eisenberg, R. Luthy, and J. U. Bowie, Methods Enzymol. **277**, 396 (1997).
[24]R. Chen, L. Li, and Z. P. Weng, Proteins: Struct., Funct., Genet. **52**, 80 (2003).
[25]P. K. Maiti and B. Bagchi, Nano Lett. **6**, 2478 (2006).
[26]P. K. Maiti and R. Messina, Macromolecules **41**, 5002 (2008).
[27]P. K. Maiti and B. Bagchi, J. Chem. Phys. **131**, 214901 (2009).
[28]W. L. Jorgensen, J. Chandrasekhar, J. D. Madura, R. W. Impey, and M. L. Klein, J. Chem. Phys. **79**, 926 (1983).
[29]J. P. Ryckaert, G. Ciccotti, and H. J. C. Berendsen, J. Comput. Phys. **23**, 327 (1977).
[30]H. J. C. Berendsen, J. P. M. Postma, W. F. Vangunsteren, A. Dinola, and J. R. Haak, J. Chem. Phys. **81**, 3684 (1984).
[31]B. Nandy and P. K. Maiti, J. Phys. Chem. B. **115**, 217 (2011).
[32]S. L. Mayo, B. D. Olafson, and W. A. Goddard, J. Phys. Chem. **94**, 8897 (1990).
[33]D. Kosztin, S. Izrailev, and K. Schulten, Biophys. J. **76**, 188 (1999).
[34]J. C. Phillips, R. Braun, W. Wang, J. Gumbart, E. Tajkhorshid, E. Villa, C. Chipot, R. D. Skeel, L. Kalé, and K. Schulten, J. Comput. Chem. **26**, 1781 (2005).
[35]I. Massova and P. A. Kollman, Perspect. Drug Discovery Des. **18**, 113 (2000).
[36]D. Sitkoff, K. A. Sharp, and B. Honig, J. Phys. Chem. **98**, 1978 (1994).
[37]W. Humphrey, A. Dalke, and K. Schulten, J. Mol. Graphics **14**, 33 (1996).
[38]D. G. Myszka, R. W. Sweet, P. Hensley, M. Brigham-Burke, P. D. Kwong, W. A. Hendrickson, R. Wyatt, J. Sodroski, and M. L. Doyle, Proc. Natl. Acad. Sci. U.S.A. **97**, 9026 (2000).
[39]B. Guo and W. H. Guilford, Proc. Natl. Acad. Sci. U.S.A. **103**, 9844 (2006).
[40]B. T. Marshall, M. Long, J. W. Piper, T. Yago, R. P. McEver, and C. Zhu, Nature (London) **423**, 190 (2003).
[41]E. Evans, A. Leung, V. Heinrich, and C. Zhu, Proc. Natl. Acad. Sci. U.S.A. **101**, 11281 (2004).
[42]Y. Suzuki and O. K. Dudko, Phys. Rev. Lett. **104**, 048101 (2010).
[43]W. L. Jorgensen, Nature (London) **466**, 42 (2010).
[44]F. Colizzi, R. Perozzo, L. Scapozza, M. Recanatini, and A. Cavalli, J. Am. Chem. Soc. **132**, 7361 (2010).
[45]S. P. Layne, M. J. Merges, M. Dembo, J. L. Spouge, and P. L. Nara, Nature (London) **346**, 277 (1990).
[46]S. E. Kuhmann, E. J. Platt, S. L. Kozak, and D. Kabat, J. Virol. **74**, 7005 (2000).
[47]See supplementary material at http://dx.doi.org/10.1063/1.4812801 for additional figures and analysis.